Characteristics of an ECR Sheet-Shaped Plasma Formed by a Combination of Permanent Magnets and Field Coils*)

Arnold Rey B. GINES and Motoi WADA

Graduate School of Science and Engineering, Doshisha University, Kyotanabe, Kyoto 610-0394, Japan

(Received 10 January 2019 / Accepted 21 March 2019)

An ECR sheet plasma device employing a 2.45 GHz microwave source and combination of permanent magnets and field coils is being developed. The combined field realized a linear magnetic field that sustained a rectilinear confinement of the plasma. The ECR condition effectively lowered the plasma ignition power to below 500 W and minimum plasma sustaining power to 94 W while also increasing the pressure range of low power ignition. Low ignition power is observed while plasma density is highest at 0.7 - 0.3 Pa pressure range. Stable plasma operation at input microwave power of up to 3 kW was achieved without overheating in the quartz window region with the aid of a gas feed mechanism on the quartz window.

Keywords: magnetized plasma, electron cyclotron resonance, sheet-shaped plasma, argon plasma, microwave plasma

DOI: 10.1585/pfr.14.3401085

1. Introduction

A weakly ionized plasma opens new ways to synthesize materials and modify surface structures [1]. Sheet plasmas have the advantage of producing thin films and functional surfaces by generating localized high-density and temperature gradient regions suitable for specific reactions. A stream of high energy electrons from a plasma cathode efficiently excites and/or ionizes atomic and molecular species which are confined in a linear magnetic field [2, 3]. The so called Uramoto-type sheet plasma device employs one of the simplest design to realize a sheet-shaped plasma by combining a linear magnetic field produced by electromagnets and a pair of dipole permanent magnets [4]. Because of the performance to create a thin plasma, the configuration was utilized among several research groups [5–7].

To realize a sheet-shaped plasma profile, a linear magnetic field is arranged such that electrons produced in the ionizing region are guided along the field line of force. Among different modes of excitation, microwave-based electron cyclotron resonance (ECR) enables excitation at lower gas pressure and lower input power while also eliminating high temperature cathodes that introduce impurities into the plasma, thereby, providing greater degrees of freedom on plasma processing parameters. A simple configuration for plasma production by ECR condition and rectangular magnetic confinement has been designed. Yoshida and Kajinishi [8] employed two coils fed by current of up to 210 A to produce a field equivalent to 1300 G along the discharge chamber and injected a 2.45 GHz microwave power through a quartz glass window. Large current to maintain the magnetic field for long operations is not ideal. Morishita *et al.* [9] employed a set of permanent magnets to produce cusp field near the cathode. While a uniform sheet plasma in the length of 20 cm is produced, the field profile is limited by the fix flux density created by the permanent magnets. Noguera and Ramos [10], and Ramos, *et al.* [11] employed a sheet plasma device with the magnetic field structure similar to the original Uramoto-type sheet to form TiN films for hard coatings. Impurity emissions from the plasma cathode often restrict usage of this type of device for any plasma process that forbids introduction of trace impurities.

We investigate the production of sheet-shaped plasma sustained in a moderate intensity magnetic field using a 2.45 GHz microwave source. A localized ECR condition is realized through combining the linear magnetic field produced by coils and a pair of permanent magnets. The discharge conditions satisfying ECR and that with the field intensity for sub-ECR conditions are reported.

2. Device Set-Up

Figure 1 illustrates the device set-up with the definitions of coordinates. A 290 mm-long stainless steel six-way cross chamber serves as the plasma container. A 2.45 GHz microwave power source, which has a maximum power output of 3 kW, delivers the electromagnetic radiation to the chamber through a tapered copper waveguide and a 110 mm by 7 mm quartz glass window. The system is evacuated by a 355 ℓ/s turbo molecular pump down to 10^{-5} Pa base pressure.

Three sets of identical pan-cake coils that are electri-

author's e-mail: euq3301@mail4.doshisha.ac.jp

*) This article is based on the presentation at the 27th International Toki Conference (ITC27) & the 13th Asia Pacific Plasma Theory Conference (APPTC2018).

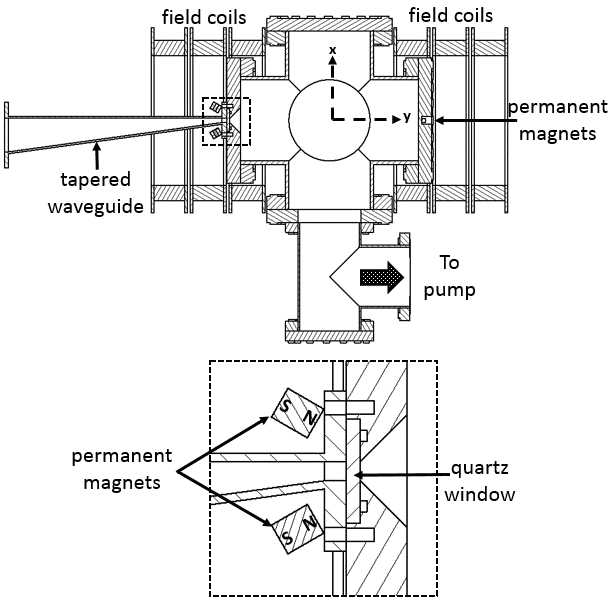

Fig. 1 Cross-section of the sheet plasma device using permanent magnets and field coils to produce a line cusp field. The inset shows details of the quartz window region.

cally connected in series produce a linear magnetic field with weak magnetic mirrors inside the vacuum chamber. The field strength produced by the coils can be adjusted by controlling the current applied on the coils from a DC source which can provide up to 15 A current. Figure 2 shows the measured field contribution of the coils along the *y*-axis inside the chamber starting from the plasma-facing side of the quartz glass. At 15 A, the field is maximum (430 G) at the quarts window. To realize resonance condition satisfying ECR at $B = 875$ G, the field is increased by installing Nd-Fe magnets in the region around the quartz microwave window. These permanent magnets generate cusp field along the *y*-axis with a maximum flux density of 480 G at the quartz window. When combined with the field coils (at 15 A), the total field generates the intensity corresponding to an ECR region just several millimeters from the quartz window along the axis of the linear magnetic field. A Hall probe coupled to a Lakeshore Model 460 3-channel gauss meter measured the field along the y-axis. The magnetic flux density profiles of the total field from the permanent magnets and the field coils along the chamber axis is also shown in Fig. 2.

Figure 3 a) shows the initial microwave inlet flange design. During plasma production, localized heating was observed in the quartz glass region despite fitting a water-cooling system on the outer face of the flange. A substantial heating was observed at non-ECR conditions. When the microwave power exceeds 1.5 kW, the microwave inlet region considerably heated up to eventually burn the high temperature O-ring seal and damaged the quartz glass. To resolve this overheating problem, a gas inlet feature is incorporated into the flange design as shown as shown in Fig. 3 b). The gas inlet structure supplies neutral gas in the

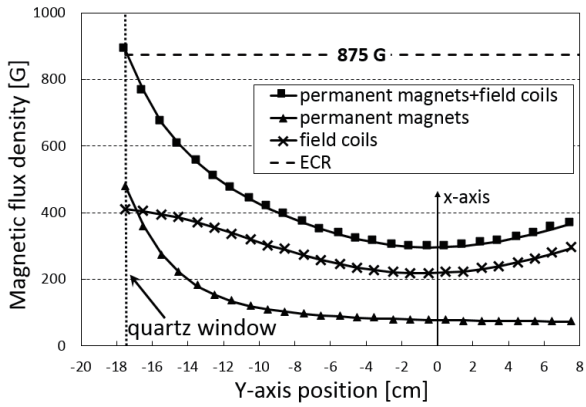

Fig. 2 Magnetic flux density profile along the downstream central axis inside the chamber. The coil current is 15 A.

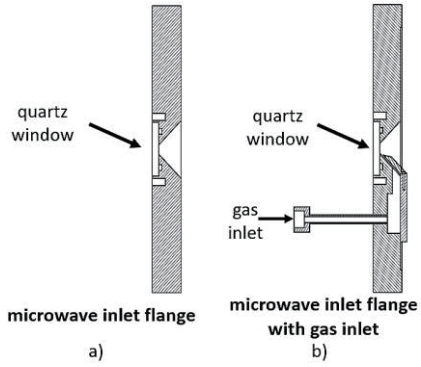

Fig. 3 Microwave inlet flange designs. a) Simple flange with quartz glass window, and b) similar flange as [a)] with gas introduction inlet.

vicinity of quartz window surface to enhance recombination for cooling down the temperature and density of the local plasma in touch with the window surface realizing the condition similar to a gas divertor [12]. This configuration can sustain plasma excited with up to 3 kW microwave power without damaging the seals and the quartz window for several minutes. The cooling mechanism enables full range of possible microwave power available during this investigation.

A Langmuir probe obtains *I* - *V* characteristics of the plasma. The cylindrical probe consists of a 0.6 mm diameter tungsten wire enveloped in an alumina tube that leaves a 2 mm exposed end tip of the wire. A grounded copper tube electrostatically shields the probe signal line from ambient noise. A larger alumina tube shields the copper tube and its contents from plasma irradiation and the probe signal noise from electromagnetic radiation in the chamber. A Yokogawa model GS610 source measure unit digitally records the *I* - *V* curve.

3. Results and Discussion

3.1 Ignition and extinction power

In Fig. 4, the ignition and extinction powers as func-

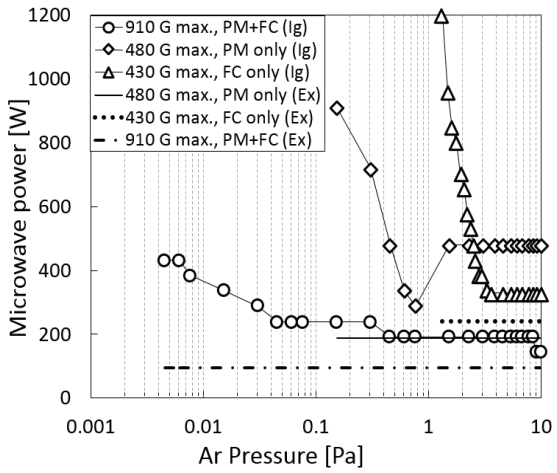

Fig. 4 Ignition (Ig) and extinction (Ex) powers at varying Ar pressure from different field geometries, namely, field coils (FC), permanent magnets (PM), and combination (PM+FC).

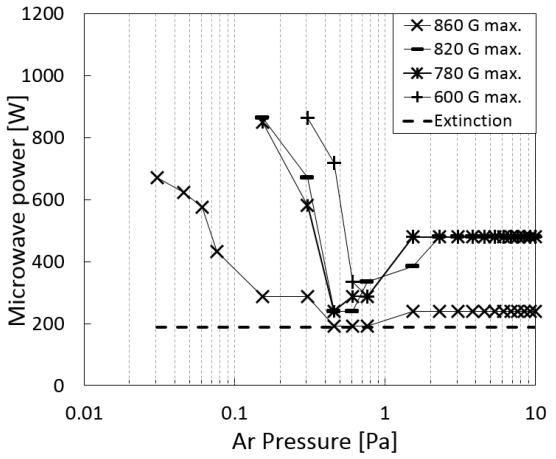

Fig. 5 Ignition and extinction powers at varying Ar pressure relative to field strength.

tions of gas pressure in the three different magnetic field geometries are shown. The microwave power was slowly increased until a stable discharge is initiated to record the ignition microwave power at the corresponding Ar pressure condition. When only the magnetic field from the field coils (FC) are present, ignition occurs at 330 W in the high-pressure range at 15 A current on FC equivalent to a maximum field of 430 G at the quartz window. The required power remains constant down to 3 Pa pressure before it starts to increase exponentially up to 1200 W at 1.3 Pa. When the Nd-Fe permanent magnets (PM) are installed in the microwave inlet region, they provide a maximum magnetic field flux of 480 G at the quartz glass surface. With only the PM inducing the magnetic field, the minimum microwave power required to commence a discharge is about 480 W and the power remains constant down to 1.5 Pa. A dip in the ignition power plot occurs at 0.7 - 0.3 Pa only to increase again up to 900 W at 150 mPa. When the fields from the permanent magnets and the coils are combined to achieve ECR condition near the inlet of the quartz microwave inlet region, ignition occurs around 190 W at high pressure and slowly increases only up to 430 W even further down to pressures less than 5 mPa. At the lowest observable pressure, when the plasma glow does not propagate across the chamber and is limited at the surface of the quartz glass, the plot is terminated. The extinction power, or the minimum power required to sustain the plasma is 240 W with coils, 188 W with magnets and only 90 W at ECR. The extinction power remains constant for each of the conditions above and is represented by the three horizontal lines in Fig. 4.

The dependence of the ignition and extinction powers to the strength of the combined fields below 875 G is illustrated in Fig. 5. The DC source of the coils was controlled to set the maximum field less than 875 G. At 4 A, the total field at the vacuum side of the quartz window surface is 600 G. The ignition power profile follows a similar behavior as when only the permanent magnets are present. This trend continues up to 12 A (820 G max.) with improved ignition towards the lower pressure range. A dip in the 0.3 - 0.7 Pa range is also present with a significant increase towards lower pressure. Close to the ECR condition at B = 860 G, there is a considerable improvement in ignition towards lower pressure down to 30 mPa at only 670 W. The extinction power remains constant at 188 W in all of the field intensities below ECR and is also shown in Fig. 5.

From the low pressure region in sub-ECR condition involving permanent magnets, a decrease in the ignition power as the pressure is increased accounts for the increase in the particle's mean free path inside the chamber as more gas is introduced into the system. As such, an increase in collision frequency promotes more efficient ionization until a minimum ignition power is attained at 0.4 - 0.7 Pa. At pressure greater than at the minimum breakdown, the ignition power is higher but remains invariable. At this point, the electron temperature decreases due to further increase in collision frequency.

Popov *et al.* [13] observed in their 2.45 GHz microwave plasma device that a reduction in the minimum ignition power occurs when the magnetic flux density is set to be greater than 430 G to which they attribute to the transition from an underdense plasma mode below 430 G to overdense plasma mode at 430 - 440 G. It is argued that the transition arise from the abrupt increase of the microwave power absorption in the resonance on the second gyrotron harmonic, $\omega = 2\omega_{ce}$ [14, 15]. The observed transition to lower power with respect to the flux density corresponds to the same range of minimum power occurrence observed from $B > 430$ G. The dip starting from $B > 430$ G manifests this transition towards the minimum power at 188 W in ECR.

3.2 Pressure dependence of plasma density

Langmuir probe measurement obtained at the center

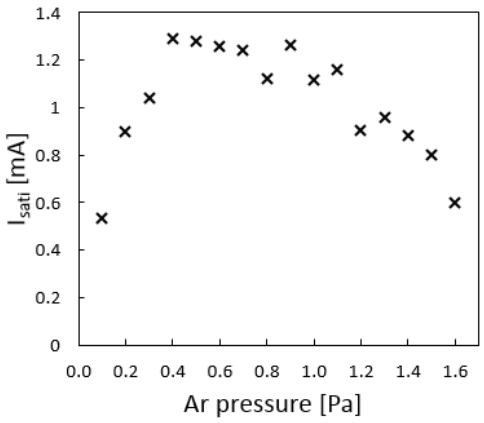

Fig. 6 Ion saturation current (I_{sati}) at varying pressure along the vacuum chamber's central axis.

of the chamber at $x = 0$, $y = 0$, around 17.5 cm from the quartz window surface along the plasma downstream, provides the ion saturation current, I_{sati}, of the Ar plasma observed at −75 V probe bias. Figure 6 shows the plot of I_{sati} relative to Ar gas pressure at fixed 1 kW microwave power. The current is highest at 0.4 - 0.9 Pa pressure range and decreases beyond this range. An estimate of the ionization mean free path, λ_{mfp}, reveals the behavior of I_{sati} relative to gas pressure. The mean free path is the inverse of the product of cross section, σ, and number density, n, or $\lambda_{mfp} = 1/\sigma n$. At 0.5 Pa gas pressure, n for argon is around 1.33×10^{14} cm^{-3} while an approximate value of the ionization cross section $\sigma = 2.5 \times 10^{-16}$ cm^2 from AMDIS database [16] for a reaction [Ar + e → Ar$^+$ +2e] is used. From here, λ_{mfp} is around 30 cm and is comparable to the device dimension. The total distance from the quartz glass surface to the opposite chamber wall is around 30.5 cm. At lower pressure, particles diffuse towards the chamber wall while recombination is favored at higher pressure.

3.3 Sheet plasma profile dependence on magnetic field

A movable stage allows for a 50 mm range of linear motion of the probe tip along the x-axis to determine the axial profile of the plasma. Several Langmuir probe scans were performed along the plasma width at 3 mm distance for each scan. Ion saturation currents (I_{sati}), electron temperatures (T_e), and electron densities (n_e) were derived from the I - V curve and are plotted in Fig. 7. Density distribution of the plasma particles and electron temperature depict the sheet plasma thickness and its behavior in the presence of varying linear magnetic field. The plasma was maintained by 2 kW microwave power at 0.5 Pa while field measurements were obtained at the center of the chamber along the probe scan direction at $x = 0$. Starting at lower field (13 A equivalent to 265 G), the axial profiles of the ion saturation current and electron density behave similarly and form a gradual gradient peaking at $x = 0$. An increase (1 A equivalent to 14 G) in the field strength

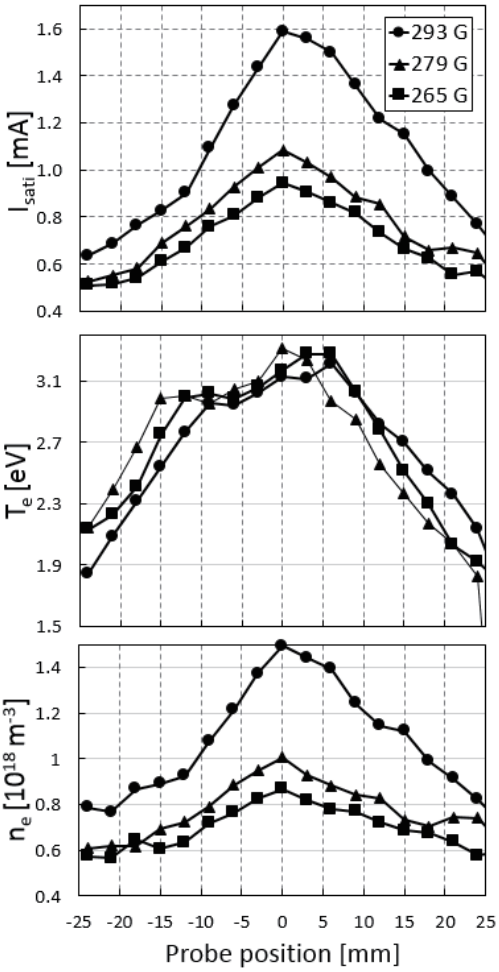

Fig. 7 Axial profiles of ion saturation current (I_{sati}), electron temperature (T_e) and of electron density (n_e) relative to magnetic field strength along the x-axis. The indicated fields were measured at position $x = 0$.

slightly elevates the gradient while maintaining the same axial profile. When the current is set at 15 A, the field at $x = 0$ is 293 G while an ECR condition is achieved near the quartz window. The ion saturation and electron density magnitudes form steeper gradient with greater magnitude increase along the center of the plasma sheet achieving electron density ~10^{18} m^{-3}. The electron temperature axial profile shows high energy electrons populating the center of the plasma. The field strength did not affect the electron temperature largely because the present treatment to determine the electron temperature is by using the low temperature Maxwell component. The ECR condition enhanced the ionization while the increase of magnetic field in sub-ECR condition did not improve sheet plasma thickness.

Previously reported sheet plasma thicknesses were defined in terms of ion Larmor radius [17,18] where the sheet thickness is described as approximately twice the mean ion Larmor radius. Gyrating ions move relative to guiding centers that lie in the vicinity of the sheet plasma midplane. Taking the condition at a pressure of 0.5 Pa and magnetic

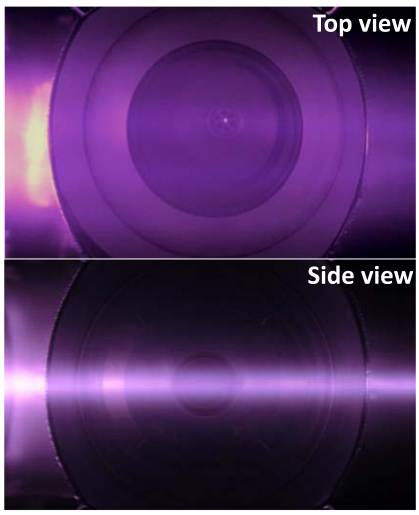

Fig. 8 Images of the sheet plasma illustrating the sheet plasma when viewed from the top (Top view) and the sheet thickness along the horizontal center of the chamber viewed on its side (Side view).

flux density $B = 293\,\mathrm{G}$, the ion Larmor radius r_i is approximately 7 mm when the ion temperature is considered to be around 0.1 eV. In the meantime, r_i can be 38 mm if we assume r_i is determined from ion acoustic velocity for 3 eV electron temperature. When compared to the half width half maximum of the plot of the radial profile of ion saturation current, the plasma thickness is around 34 mm. Figure 8 shows the sheet plasma at the same condition when viewed from the top (Top view) and on its side (Side view). The second image reveals the plasma thickness based from the observed plasma glow along the midplane. As reference, the circular profile at the center of the image has a 37 mm diameter. This implies that the plasma has a thickness less than this value which is comparable to the estimate of its full width half maximum value at around 34 mm. Clearly, the observed plasma thickness is less than twice the expected plasma thickness when compared with the calculated ion Larmor radius.

4. Conclusion

A new sheet plasma device employing a combination of field coils and permanent magnets has been designed and operated. The design includes a gas feed system that cools the quartz window surface allowing plasma operation at microwave power up 3 kW without damaging the quartz glass microwave inlet structure. The field strength raises the plasma density while ECR condition significantly enhances plasma production to attain electron density to $10^{18}\,\mathrm{m}^{-3}$ range. The electron temperature of the bulk plasma remains independent of the magnetic field strength.

[1] S. Dou, L. Tao, R. Wang, S.E. Hankari, R. Chen and S. Wang, Adv. Mater. **30**, 1705850 (2018).
[2] M. Wada, S. Takeshima, H. Tsuda and M. Sasao, Rev. Sci. Instrum. **61**, 430 (1990).
[3] Y. Abate and H.J. Ramos, Rev. Sci. Instrum. **71**, 3689 (2000).
[4] J. Uramoto, Shinku (in Japanese) **25**, 719 (1982).
[5] K. Jimbo and M. Iima, Rev. Sci. Instrum. **66**, 1035 (1995).
[6] K. Nakase, T. Shibata, T. Yasui, H. Tahara and T. Yoshikawa, Thin Solid Films **281-282**, 152 (1996).
[7] K. Shibata, N. Yugami and Y. Nishida, Rev. Sci. Instrum. **65**, 2310 (1994).
[8] M. Yoshida and K. Kajinishi, IEEE Trans. Plasma Sci. **31**, 40 (2003).
[9] N. Morishita, S. Ishii, Y. Kato, F. Tani, Y. Koizumi and M. Sunagawa, Proceedings of 11th International Conference on Ion Implantation Technology **2**, 752 (1998).
[10] V.R. Noguera and H.J. Ramos, Thin Solid Films **506-507**, 613 (2006).
[11] H.J. Ramos, K. Doi, M.S. Fernandez, G.M. Malapit, M. Sasao, M.M.S. Villamayor and M. Wada, JPS Conf. Proc. **1**, 015060 (2014).
[12] J.W. Davis, D.E. Driemeyer, J.R. Haines and R.T. McGrath, J. Nucl. Mater. **212-215**, 1353 (1994).
[13] O.A. Popov, S.Y. Shapoval and D.Y. Yoder Jr., Plasma Sources Sci. Technol. **1**, 7 (1992).
[14] T. Stix, *Waves in Plasmas* (Springer-Verlag, New York, 1992) p. 270.
[15] J. Datlov, J. Teichman and F. Zacek, Phys. Lett. **17**, 30 (1965).
[16] AMDIS ionization database, NIFS database, Japan National Institute of Fusion Science.
[17] K. Sukani, K. Nanri, T. Noguchi, E. Yabe and K. Takayama, Nucl. Instrum. Methods Phys. Res. B **111**, 151 (1996).
[18] Y. Okuno, H. Ishikura and H. Fujita, Rev. Sci. Instrum. **63** (7), No. 7, 3725 (1992).